Clay Minerals, (2015) **50**, 353–367

Surface structure of organoclays as examined by X-ray photoelectron spectroscopy and molecular dynamics simulations

B. SCHAMPERA[1,*], R. SOLC[2], S. K. WOCHE[1], R. MIKUTTA[1], S. DULTZ[1], G. GUGGENBERGER[1] AND D. TUNEGA[2]

[1] *Institute of Soil Science, Leibniz Universität Hannover, Herrenhäuser Straße 2, D-30419 Hannover, Germany*
[2] *Institute for Soil Research, University of Natural Resources and Life Sciences Vienna, Peter Jordan-Straße 82, A–1190, Austria*

(*Received 11 December 2014; revised 21 April 2015; Guest Editor: M. Plötze*)

ABSTRACT: Organoclays are sorbent materials prepared from clays by exchanging inorganic with organic cations. Their properties depend on the loading and conformational structure of the organic cations, but little information is available about the surface structures of organoclays. In this work, X-ray photoelectron spectroscopy (XPS) and classical molecular dynamics (MD) simulations are combined to characterize the external interface of an organoclay prepared from hexadecylpyridinium ($HDPy^+$) and bentonite. The XPS survey spectra show well the varying elemental composition of the surface with increasing amount of surfactant, showing a decreasing contribution of clay-derived elements with increasing organic coverage. The high-resolution C 1s XPS spectra depict sensitively the surface arrangement of the surfactant. In combination with MD simulations, the results implied a monolayer coating for low surfactant coverage and a disordered bilayer arrangement at high surfactant uptakes. Molecular dynamics simulations showed that for very high cation uptake a quasi-paraffin-like configuration is also possible. The combination of experimental and modelling methods yielded congruent information on the molecular-scale arrangement of organic cations at the organoclay surfaces and the controlling mechanisms.

KEYWORDS: organoclay, surface arrangement, XPS, molecular dynamics.

Organoclays are organically modified clays having specific material properties such as selective sorption properties for anions or non-polar compounds. They can be used, therefore, for a variety of environmental applications, e.g. in waste-water treatments or as barrier materials for waste deposits (Yariv, 2002; Rytwo *et al.*, 2012). During organoclay preparation, exchangeable inorganic cations from interlayer and external clay surfaces are exchanged by organic cationic surfactants, usually amphiphilic alkylammonium cations such as hexadecylpyridinium ($HDPy^+$) or hexatrimethylammonium ($HDTMA^+$). This is the first step during which the sorption capacity of clays for anions and organic molecules is often increased (Park *et al.*, 2013). The replacement of the small inorganic cations by large organic cations results in substantial structural changes and, consequently, also in physical properties, e.g. wettability, diffusion and permeation transport (Rytwo *et al.*, 2005; Schampera & Dultz, 2009). These properties can be modified by careful selection of the clay mineral, the organic surfactant and the loading of the organic cation chosen.

The basic transport process in porous media which controls pollutant displacement in barriers of saturated compacted clays is diffusion and this is because of the large swelling capacity induced by low hydraulic

* E-mail: schampera@ifbk.uni-hannover.de
DOI: 10.1180/claymin.2015.050.3.08

conductivity of water. The transport mechanism is generally affected by material-surface composition and properties (Shackelford & Moore, 2013). Therefore, the understanding of the interfacial interactions, structural arrangement and conformation in the hybrid organoclay systems, specifically at a nanoscale level, is of utmost importance in predicting their environmental behaviour and assessing possible applications.

Numerous experimental studies have been devoted to the arrangement of organic cations in the clay interlayer space, where the response of clay interlayers to applied organic cations has been investigated by X-ray diffraction (XRD; Koh *et al.*, 2005; He *et al.*, 2006, 2014), thermal gravimetric analysis (TGA; Dultz & Bors, 2000; He *et al.*, 2005, 2010), infrared (IR) spectroscopy (Dultz *et al.*, 2005; Park *et al.*, 2013), transmission electron microscopy (TEM) (Lee & Kim, 2002; Sun *et al.*, 2013), or scanning electron microscopy (SEM) (Lee & Kim, 2002; Schampera & Dultz, 2009). Moreover, molecular modelling studies of organoclays have been conducted in order to understand the structure of the interlayer space, i.e. the distribution, arrangement, interactions and chain conformations of the organic cations confined in the interlayer space of smectites (Zeng *et al.*, 2004; Meleshyn & Bunnenberg, 2006; Heinz *et al.*, 2007, 2008; Fu & Heinz, 2010; Park *et al.*, 2011; Zhao & Burns, 2012, 2013). The reliability of the simulation results depends heavily on the structural and chemical simplifications of the models, however, and also on the quality of the empirical (Force-Field, FF) parameters used, especially for a description of organic–inorganic interactions between the organic cations and clay-mineral layers.

Although there are many experimental studies that have provided information on the structural characterization and various physicochemical properties of the organoclays, less attention has been paid to the characterization of the external surfaces of organoclay particles. The external surfaces of organoclays and their charge distribution are particularly important for interfacial processes and can represent a crucial factor in controlling transport processes of environmentally hazardous chemicals through barriers containing organoclays. Typically, potentiometric titration and contact angle (CA) measurements provide information about the surface-charge distribution and the wetting properties of clay and organoclay surfaces, respectively. Depending on the loading of the clay with organic cations, the wettability as well as the net charge of organoclays can be modified extensively, including complete charge reversal from negative to positive with increasing coverage of organic cations (Schampera & Dultz, 2009). Advanced microscopic techniques such as SEM, TEM or atomic force microscopy (AFM) (Lee *et al.*, 2005; He *et al.*, 2006; Li *et al.*, 2006; Sun *et al.*, 2013), in spite of being useful in morphological characterization, provide little insight into the arrangement and binding mode of organic cations at the clay surface mostly because of the small particle size. In contrast, XPS is a very promising surface-sensitive tool for detailed surface characterization as it provides quantitative data on the elemental composition, as well as chemical, electronic and binding states of elements in the outermost surface layers. Recent XPS studies on organoclays largely addressed cation-exchange processes in the interlayer (He *et al.*, 2007; Naranjo *et al.*, 2013; Park *et al.*, 2013; Bilgic *et al.*, 2014) or the arrangement of organic cations in organoclay films (Toma *et al.*, 2010). These studies traced changes of elemental composition with respect to the organic cations in the clay interlayer mainly by XPS survey scans. Using XPS element scans, Park *et al.* (2013) analysed organoclay interlayers and observed a gradual increase of the C 1s binding energy (BE) for the C–C bond but no changes for the C–N bond of $HDTMA^+$. This observation was attributed to the changing arrangement of the organic molecules in the interlayer. Toma *et al.* (2010) investigated coatings of organic cations on clay for specific prepared films and found large differences in Al (2p, 2s) and Si (2p, 2s) BE values, attributed to a variation of organic cation coating, but no changes for the C 1s BE.

In the present work an XPS study of organoclays prepared from natural bentonite and hexadecylpyridinium choride (HDPyCl), frequently used for the preparation of organoclays, is presented. The main objective was to characterize the external organoclay interface and to identify conformational changes induced by $HDPy^+$ as a function of the surfactant loading. The XPS study was complemented by MD simulations of the organoclay models in order to achieve a molecular-scale description of the arrangements of the organic cations on the external clay surfaces.

MATERIALS AND METHODS

Source materials and organoclay preparation

Na-bentonite (MX-80, Wyoming) was purchased from AMCOL, Winsford, England. The cation exchange capacity (CEC) as determined by the

https://doi.org/10.1180/claymin.2015.050.3.08 Published online by Cambridge University Press

Ag-thiourea method was 1.003 ± 0.010 cmol/kg (Van Reeuwijk, 2003) and the BET specific surface area (SSA) derived from N_2 gas adsorption at 77 K was 26.2 m^2/g. More than 90% of the bentonite consisted of montmorillonite with a chemical composition $(Na,Ca)_{0,33}(Al_{1,67}Mg_{0,33})Si_4O_{10}(OH)_2 \bullet nH_2O$ (AMCOL, Winsford, England). Analysis-grade hexadecylpyridinium chloride monohydrate ($HDPyCl \bullet H_2O$; Fluka AG, Switzerland) was used for the preparation of the organoclay. The organoclay samples were prepared by dispersing the clay powder in deionized water prior to adding solutions with $HDPy^+$ cations corresponding to 40, 100, 120 and 200% of the CEC of the clay. The solid:solution ratio (wt.:vol.; clay/organoclay:water) always remained constant at 1:10. Samples were shaken at 6 rpm for 20 h in the dark at 22 ± 2°C in an overhead shaker. After equilibration, the excess un-adsorbed organic cations were removed by vacuum filtration using 0.45 µm cellulose acetate filters (Sartorius Stedim Biotech GmbH, Göttingen, Germany) and the organoclay recovered was rinsed three times with doubly deionized water. Finally, the samples were freeze-dried and homogenized gently. The amount of organic cations taken up by the clay was calculated from triplicate carbon measurements by a CNS-analyzer (Vario EL, Elementar Analysensysteme GmbH, Germany). The uptake of $HDPy^+$ was not fully quantitative. The samples discussed in the text below are labelled according to the organic cation content measured as HDPy-32, HDPy-93, HDPy-111 and HDPy-180, corresponding to the applied $HDPy^+$ concentration of 40, 100, 120 and 200% of the bentonite CEC.

Particle charge and contact-angle measurements

The surface charge was measured in triplicate by a particle-charge detector (PCD 03, Mütek, Herrsching, Germany) according to Böckenhoff & Fischer (2001). Briefly, 0.01 g of organoclay was suspended in 10 mL of doubly deionized water and poured into a Teflon® cup. The surface charge was determined quantitatively by titration with a charge-compensating polyelectrolyte to the point of zero charge (DL25, Mettler Toledo, Gießen, Germany). The cationic polyelectrolyte Poly-DADMAC (poly-diallyldimethylammonium chloride) was used to measure negative surface charge, whereas the anionic polyelectrolyte PES-Na (sodium polyethylene sulfonate) was applied to assess positive surface charge. The initial bentonite suspension was slightly alkaline (pH 8.1–9.8).

The wettability of the samples was analysed in terms of contact angle (CA) with the sessile drop method (SDM) using a CCD-equipped contact angle microscope (OCA 15, DataPhysics, Filderstadt, Germany) according to Bachmann *et al.* (2013). The clay sample was fixed as a thin layer on a microscopic slide with double-sided adhesive tape and a 3 µL drop of deionized water was placed on top. The initial CA, directly after placement, was determined by drop-shape analysis and fitting tangents to both sides of the drop using the software *SCA20* (DataPhysics, Filderstadt, Germany). All measurements were performed at least in triplicate.

X-ray photoelectron spectroscopy

The XPS analysis was carried out to determine the surface chemical composition of organoclays using an Axis Ultra DLD instrument (Kratos Analytical, Manchester, UK). Bombardment of the surface with X-rays (monochromated AlKα radiation, 1486.6 eV) results in the emission of photoelectrons with element-specific binding energy (BE). Owing to the inelastic mean free path, photoelectrons contributing to element peaks mainly originate from a depth of 10–30 Å with a minor contribution of photoelectrons emitted from greater depths (<100 Å) at higher energies (Tanuma, 2003). For the measurement, samples were fixed on a sample bar with ultrahigh vacuum-stable carbon conductive tape (Agar Scientific, Elektron Technology, UK Ltd., Stansted, UK) with a sample area of ~1 cm^2. At three analysis points per sample, each covering an area of 300 µm × 700 µm, the following measurements were performed. First, survey spectra in an energy range of 1200–0 eV were recorded at a resolution of 1 eV by using three sweeps, a dwell time of 500 ms and a pass energy of 160 eV. Second, detailed C 1s spectra were recorded in a range of 300 to 277 eV with a resolution of 0.1 eV by applying three sweeps, a dwell time of 300 ms and pass energy of 20 eV. The take-off angle was 0° and the emission current and high voltage were set to 20 mA and 15 kV, respectively. Despite the fact that the neutralizer was active during measurements, complete charge compensation was not always possible and the BE for all spectra had to be corrected. As Si occurred only in the clay-mineral structure and did not undergo any changes in binding status during the preparation of the organoclays, the Si 2p peak was corrected to 103 eV (Si–O bond; Toma *et al.*, 2010). The survey spectra have been quantified in terms of atomic % (at.%) for the elements identified using the software

https://doi.org/10.1180/claymin.2015.050.3.08 Published online by Cambridge University Press

Vision 2 (Kratos Analytical, Manchester, UK). In addition, the three survey scans per sample were normalized to the intensity of the O 1s peak to create the mean spectrum. The O 1s peak was chosen because the oxygen present in the clay structure does not change during the exchange of cations. A peak deconvolution of the C 1s scans was done using the *UNIFIT 2010* software (Hesse *et al.*, 2002). Fitting of C–C and C–N subpeaks (He *et al.*, 2007) as present in $HDPy^+$ was performed using a symmetric Gaussian–Lorentzian cross-product function (0.5 mixing) after a Shirley background subtraction of the baseline. Best fits were obtained once the binding energies (BE) were initially allowed to vary between 280 and 284 eV (C–C) and 284 and 290 eV (C–N). Likewise, initial full width at half maximum (FWHM) values were not constrained; the average final FWHM values were 1.75 ± 0.07 and 1.95 ± 0.18 for the C–C and C–N subpeaks, respectively.

MD simulations

Models of the external organoclay surfaces were built on the basic model of a single montmorillonite layer derived from a Wyoming-type structure having a formula unit $Na_{0.75}(Si_{7.75}Al_{0.25})(Al_{3.25}Fe_{0.25}Mg_{0.5})O_{20}(OH)_4$. For this composition, the theoretical CEC is 1.03 cmol/kg, which is close to the measured CEC of the bentonite used (1.003 cmol/kg). The basal surface of the single model layer is a dominant (001) surface of montmorillonite particles that are usually irregularly shaped, thin platelets of <1 μm in size. The initial computational cell consists of eight unit cells with a lateral 4*a*–2*b* cell dimension of 20.65 Å × 17.96 Å (*a* and *b* are the original unit-cell vectors) and this size and isomorphic substitutions lead to a cation coverage of three Na^+ ions per surface (i.e. the CEC of this layer model). To construct models of the external organoclay surfaces reflecting the increasing coverage by the organic cations, an increasing number of $HDPy^+$ ions was placed on the surface of the single montmorillonite layer. In total, eight models were prepared. For low surface concentrations (<100% of CEC), Na^+ cations were replaced by $HDPy^+$ cations having positively charged heads located directly at the original Na^+ positions. Aliphatic tails (in all-*trans* conformation) of the initial cation arrangements have a perpendicular orientation towards the clay surface. For a low uptake of the organic cations, with only up to four cations in the 4*a*–2*b* computational cell, a monolayer arrangement is assumed where all positively charged heads are near the surface (models HDPy_1–HDPy_4; which corresponds to a $HDPy^+$ uptake of 33–133% of the CEC; Table 1). Models with more than four $HDPy^+$ ions per computational cell assume a bilayer arrangement of organic cations with only even numbers of $HDPy^+$ being considered (200–400% of the CEC). Here, half of the organic cations were placed with their head groups towards the montmorillonite surface whereas the other half was oriented in the opposite direction. In total, four models with a bilayer arrangement were constructed (models HDPy_(6, 8, 10, 12); Table 1). In the case of models with the number of the cations exceeding the total layer charge per surface (models with more than three $HDPy^+$ ions) the overall positive charge was compensated by adding a corresponding amount of chloride anions placed near the positively charged heads of the cations. Finally, the models constructed in this way were then expanded two times in the *a* and *b* directions to form final simulation cells with dimensions of 43.30 Å × 35.92 Å. In all models a vacuum was added above the surface resulting in the *c* cell vector of 122.73 Å. During the calculations, periodic boundary conditions were used in all dimensions. The MD simulations were performed using the LAMMPS simulation package (Plimpton, 1995). The interactions between surface, organic cations and chloride anions were described using *CLAYFF* (Cygan *et al.*, 2004) and *OPLS–AA* (Jorgensen *et al.*, 1996) force fields.

To obtain trajectories, the Newton equations of motion were integrated numerically using the Verlet velocity algorithm with a time step of 1.0 fs. The short-range van der Waals and coulombic interactions were truncated using 12.0 Å and 17.0 Å cutoffs, respectively. Long-range coulombic electrostatic interactions

TABLE 1. HDPy_x models used in MD simulations with 'x' representing the number of organic cations on the clay surface in a computational cell with cell vectors *a* = 20.65 Å and *b* = 17.96 Å.

	x	% of CEC
monolayer	1	33
	2	67
	3	100
	4	133
bilayer	6	200
	8	267
	10	333
	12	400

https://doi.org/10.1180/claymin.2015.050.3.08 Published online by Cambridge University Press

were computed using the Particle-Particle Particle-Mesh (PPPM) method (Hockney & Eastwood, 1988). During the simulations, the montmorillonite surface was kept rigid; only the intralayer hydroxyl groups were allowed to move. The movement of the atoms from the solid montmorillonite layer is much smaller compared to movement of the flexible organic cations at the surface. Therefore, using rigid atoms of the montmorillonite layer saves computational time by excluding them from time integration but pairwise interactions are still included. This approach is used frequently in the MD simulations of solid surfaces interacting with molecular species or liquid (e.g. water) slabs (Klebow & Meleshyn, 2012). As a first MD phase, an equilibration in the canonical *NVT* ensemble (constant number of particles (N), volume (V) and temperature (T)) was performed. This phase started at 350 K and the system was cooled to 300 K within 1 ns. Then, the system was further equilibrated for 5 ns at 300 K. The last configuration from the equilibration phase was taken as an initial configuration for the production phase. The application of a protocol with a higher initial temperature and following cooling to the desired temperature was used as an accelerating equilibration phase to achieve a better mapping of the configurational space. Several temperatures and cooling protocols were tested and the initial temperature of 350 K was found to be optimal for the faster equilibration of the modeled systems. The simulation was performed using the *NVT* ensemble in a time period of 5 ns. During all simulations the temperature was controlled using a Nosé–Hoover thermostat (Hoover, 1985). The MD snapshots were recorded every 10 ps and analysed in terms of one-dimensional density profiles of the atomic positions of the selected atoms in a direction perpendicular to the montmorillonite layer surface. The block averaging scheme was used to check the stability of the temporal evolution of the potential energy of the systems. This analysis confirmed that a production phase of 5 ns is enough for the calculation of the one-dimensional density profiles. To illustrate, Fig. 1 displays a temporal evolution of the relative potential energy, U_{rel}, for the HDPy_10 model during the production phase. The evolution is stable, with energy fluctuations within the range of ±100 kcal/mol. The other models showed very similar trends in the temporal evolution of the potential energy.

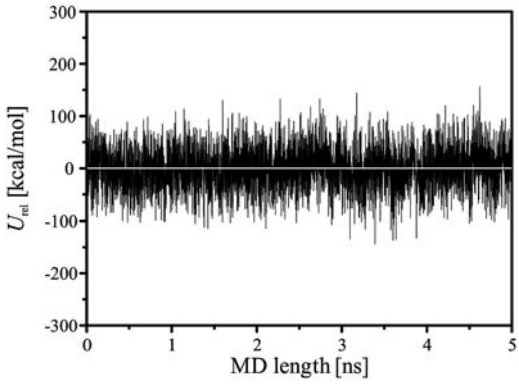

FIG. 1. Temporal evolution of the relative potential energy for the model HDPy_10 during the production phase.

In an organoclay prepared in the laboratory, e.g. HDPy-montmorillonite, 1.8% of residual water was detected (Dultz *et al.*, 2005). This amount can only have a tiny impact on the distribution of the organic cation coating. It is thus expected that this water has no effect on the orientation of the organic cations on the surfaces. The models used in the MD simulations did not include residual water molecules, therefore.

RESULTS AND DISCUSSION

Organoclay characteristics

In the organoclay samples the smectite interlayer space was expanded from 14.0 to 20.5 Å with increasing cation loadings. This increase mirrors the interlayer transition of organic cations from mono- through bi- to pseudotrimolecular structure (Schampera & Dultz, 2009, 2011). The changes in the interlayer arrangement with respect to the increasing amount of cations were described successfully by Monte Carlo simulations with a good correlation between model and experimental data (Meleshyn & Bunnenberg, 2006). With increasing cation content, the surface charge showed a steady change of the negatively charged surface (–118.7 cmmol/kg) of the natural clay to a highly positive value (214.0 cmmol/kg) for the sample with the greatest $HDPy^+$ loading (Table 2). The contact angle varied from 17 to 96°, with a hydrophobic surface (CA >90°) arising at near-neutral net surface charge, which was the case for samples with a medium uptake of organic cations (71 and 93% of the CEC; Table 2). For high cation loadings (≥106% of the CEC), the organoclay surfaces showed again a greater affinity for water (Schampera & Dultz, 2009, 2011). As wettability is controlled by the surface properties (structure and composition) a variable distribution of organic cations on the surface can be deduced. In particular, a hydrophobic surface is

https://doi.org/10.1180/claymin.2015.050.3.08 Published online by Cambridge University Press

TABLE 2. Amount of organic cations in terms of % of CEC, surface charge and contact angle, of the organoclay samples prepared.

$HDPy^+$ [% of CEC]	Surface charge [$mmol_c/kg$]	Contact angle [°]
0	118.7 ± 6.6	53 ± 6
16	19.3 ± 0.3	110 ± 24
32	n.a.	n.a.
71	17.4 ± 3.2	91 ± 21
93	13.6 ± 1.7	96 ± 19
106	4.5 ± 0.7	67 ± 11
111	n.a.	n.a.
157	54.7 ± 16.0	17 ± 7
180	181.8 ± 35.5	56 ± 11
222	214.0 ± 9.4	35 ± 6

n.a. = not analysed.

induced by the aliphatic chains of $HDPy^+$ in the monomolecular arrangement of the cations.

XPS measurements – survey scans

The surface elemental composition of the smectites showed a Si:Al ratio of 3:1 and an O content of 57.17 at.% (Table 3), which is typical for the silicate layer of montmorillonite (Mravcakova *et al.*, 2006; Biglic *et al.*, 2014). With an increasing amount of the organic cations, the contribution of C increased steadily (Fig. 2a), which suggests an increasing coverage by the organic cations. This was mirrored by a parallel increase of N and Cl, which also originated from the organic cation (Fig. 2b). The increasing presence of organic cations at the clay surfaces was also reflected by the negative linear correlation between the C and O contents (Fig. 3). Similar correlations were observed also for C and Si and between C and Al (data not shown). The Na^+ concentration at the outermost clay surfaces declined with increasing organic cation loading as it was exchanged by $HDPy^+$ (Fig. 2). In the case of the first sample with the smallest amount of cation uptake (16% of CEC), the amount of Na^+ decreased markedly but its content at the surface remained relatively high (0.65 ± 0.1 at.%), suggesting a partial replacement of Na^+ by organic cations. For the other samples, with greater organic cation loading, the Na^+ was almost eliminated (Table 3), thus confirming a complete exchange of cations at the external clay surfaces.

TABLE 3. Element content of surfaces of natural clay and organoclays as derived from XPS survey scans (at.%).

	Clay	HDPy 16	HDPy 32	HDPy 71	HDPy 93	HDPy 106	HDPy 111	HDPy 157	HDPy 180	HDPy 222
Na 1s	0.97 ± 0.14	0.65 ± 0.10	0.10 ± 0.10	0.05 ± 0.04	0.02 ± 0.04	0.04 ± 0.04	0.07 ± 0.05	0.03 ± 0.03	0.03 ± 0.03	0.01 ± 0.01
Fe 2p	0.75 ± 0.13	0.59 ± 0.07	0.56 ± 0.11	0.55 ± 0.06	0.40 ± 0.00	0.41 ± 0.02	0.30 ± 0.19	0.21 ± 0.05	0.28 ± 0.18	0.30 ± 0.10
O 1s	57.71 ± 4.14	55.63 ± 2.27	47.61 ± 1.47	42.70 ± 0.51	39.03 ± 1.41	33.05 ± 0.99	28.97 ± 1.41	23.55 ± 0.91	23.33 ± 0.51	22.13 ± 0.76
N 1s	0.08 ± 0.09	0.40 ± 0.10	0.46 ± 0.18	1.21 ± 0.19	1.12 ± 0.23	1.73 ± 0.28	1.87 ± 0.47	2.05 ± 0.14	2.15 ± 0.17	2.09 ± 0.40
Ca 2p	0.69 ± 0.09	0.76 ± 0.10	0.47 ± 0.11	0.40 ± 0.05	0.27 ± 0.05	0.31 ± 0.08	0.21 ± 0.06	0.30 ± 0.09	0.21 ± 0.08	0.30 ± 0.04
C 1s	17.14 ± 7.67	18.92 ± 3.25	31.63 ± 2.62	36.66 ± 0.99	43.65 ± 2.35	48.59 ± 1.15	55.32 ± 1.67	61.52 ± 1.65	62.48 ± 0.61	63.27 ± 1.07
Cl 2p	0.03 ± 0.04	0.11 ± 0.04	0.08 ± 0.11	0.04 ± 0.03	0.10 ± 0.05	0.67 ± 0.08	0.69 ± 0.08	1.26 ± 0.14	0.99 ± 0.09	1.26 ± 0.10
Si 2p	15.44 ± 2.43	15.93 ± 0.67	13.12 ± 0.80	12.83 ± 0.21	10.57 ± 0.39	10.38 ± 0.26	8.58 ± 0.41	7.45 ± 0.38	7.01 ± 0.28	7.20 ± 0.10
Mg 2s	0.99 ± 0.15	0.76 ± 0.03	0.72 ± 0.18	0.36 ± 0.22	0.44 ± 0.01	0.42 ± 0.05	0.48 ± 0.17	0.45 ± 0.09	0.40 ± 0.07	0.31 ± 0.04
Al 2p	6.19 ± 0.96	6.25 ± 0.29	5.24 ± 0.41	5.18 ± 0.05	4.39 ± 0.42	4.40 ± 0.23	3.51 ± 0.27	3.17 ± 0.30	3.13 ± 0.25	3.14 ± 0.13
SUM	100.0	100.0	99.99	100.0	99.99	100.0	100.0	99.99	100.0	100.0

https://doi.org/10.1180/claymin.2015.050.3.08 Published online by Cambridge University Press

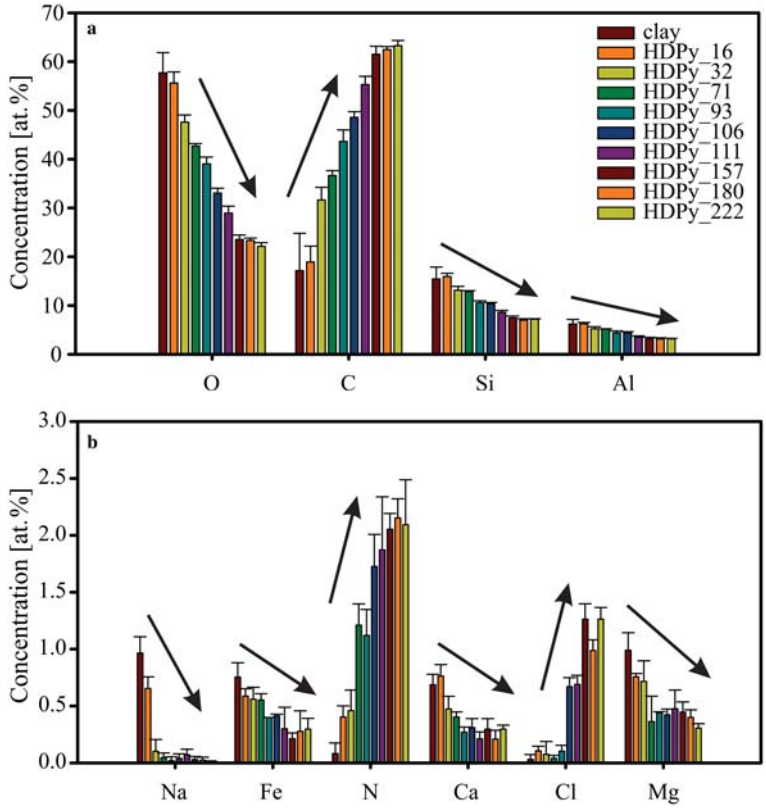

FIG. 2. Elemental content of surfaces of natural clay and organoclays as derived from XPS survey scans (at.%).

In the natural clay sample, Ca^{2+} accompanies Na^{+} cations in the interlayer space and/or surface. For small amounts of organic cations (up to 32% of the CEC) it was mostly Na^{+} which was exchanged while at higher loadings, the Ca^{2+} cations were also involved in the exchange process. However, even at the highest $HDPy^{+}$ loading, Ca^{2+} could still be detected. The residual Ca^{2+} could be explained by the presence of $CaCO_3$ in the natural bentonite. The small quantities of Mg and Fe detected originated predominantly from the smectite structure as suggested by the close correlations between their atomic concentrations and those of O in organoclay samples (data not shown). The amount of Cl^{-} increased notably for the organoclay samples at organic cation loading >100% of the CEC (Table 3). Sample HDPy-93 is a case in point because it showed a minimum content of both Na and Cl. Hence, in this sample the surface Na^{+} cations were fully replaced by organic cations but there were no excess organic cations, where the positive charge had to be neutralized by Cl^{-}.

A certain shift of BE was observed for some elements, indicating changes in the cation configuration or the character of interactions. Most prominently, BE shifts occurred for N 1s, C 1s and Cl 2p peaks for organoclays as illustrated in Fig. 4. The surface arrangement and also the interactions of the organic cations with the silicate surface layer varied with increasing amount. As outlined above, the interactions of the cations are multiple and comprise interactions with the clay surface and Cl^{-} anions anchored in the organic layer (predominantly electrostatic forces) and also their mutual dispersive interactions (between the C chains of organic cations). To further elucidate these interactions, a detailed analysis of the C 1s peak was performed.

High-resolution XPS C 1s spectra

The HDPy-derived C 1s peak was analysed by decomposing it into two sub-peaks corresponding to aliphatic C–C (at 284.90 ± 0.07 eV) and C–N

https://doi.org/10.1180/claymin.2015.050.3.08 Published online by Cambridge University Press

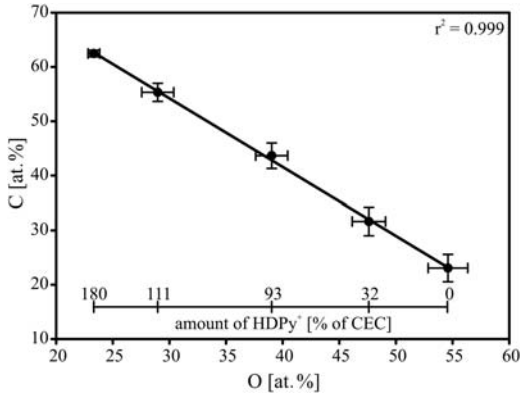

FIG. 3. Correlation between C and O at.% concentrations determined by XPS survey scans. The organic cations content in the organoclay samples increases from right to left.

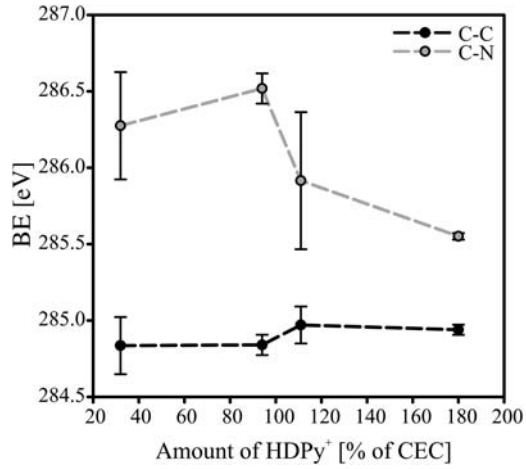

FIG. 5. Variation of C 1s binding energy deconvoluted into C–C (at 284.90 eV) and C–N bonds (at 286.06 eV) with increasing amounts of HDPy cations in the organoclay samples.

bondings (at 286.06 ± 0.42 eV). Each of these two peaks also includes signals attributable to double C=C and C=N bonds intersecting extensively the signals of the single bonds. This is because differences between the respective BE values of the saturated and non-saturated bonds are minimal (0.5–0.7 eV; Jagst, 2010). The BE assigned to the C–C bond varied only slightly in a range of 284.84 to 284.97 eV within the organoclays (Fig. 5). This means that the single C–C bonds in the aliphatic 16-C chains are only minimally affected by the interactions of the organic cations with external clay surfaces. Nevertheless, a certain difference was observed between the samples with a small *vs*. large organic cation uptake (32 and 94 *vs.* 111 and 180% of the CEC; Table 4). It was observed from MD simulations (see discussion below) that in the case of the low uptake, the organic cations form a thin monomolecular coating on the surface and their aliphatic chains are in a parallel orientation to the surface (Fig. 6). Therefore, these chains interact weakly, predominantly with the clay surface. With increasing cation loading, the organic cations start to form more complicated surface coatings, i.e. a second disordered layer of aliphatic chains with varying conformations begins to form. Finally, for the greatest cation loading, a disordered paraffin-like arrangement is formed where dispersive interactions among aliphatic chains are dominant. Thus, the observed changes of the C 1s BE of the C–C bond (Figure 5) can be attributed mainly to the change of the local environment of the cations in different orientations as

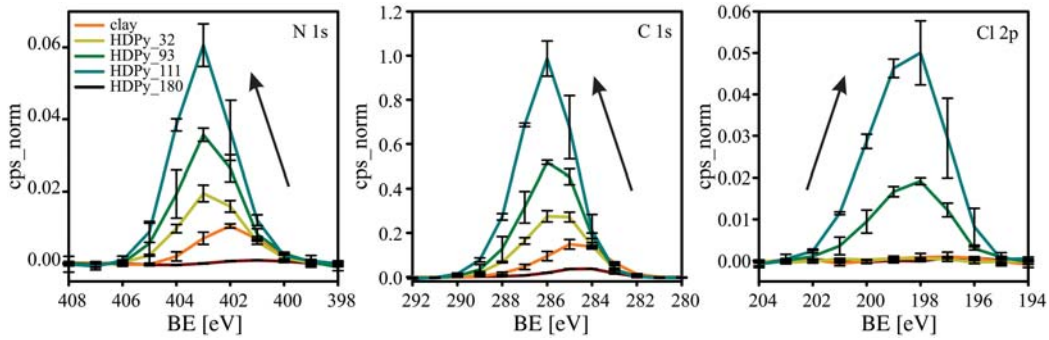

FIG. 4. Survey scans of HDPy-montmorillonite (normalized to O 1s). A shift of binding energies of N 1s and C 1s to higher BE values and Cl 2p to lower BE values is depicted by the arrows.

https://doi.org/10.1180/claymin.2015.050.3.08 Published online by Cambridge University Press

TABLE 4. Peak maxima of C–C (at 284.90 eV) and C–N (at 286.06 eV) peaks derived from deconvolution of the C 1s principal peak.

$HDPy^+$ [% of CEC]	CC [eV]	St. dev.	FHWM [eV]	St. dev.	CN [eV]	St. dev.	FHWM [eV]	St. dev.
32.00	284.84	0.19	1.83	0.15	286.27	0.35	2.16	0.22
94.00	284.84	0.07	1.88	0.05	286.52	0.10	2.29	0.52
111.00	284.97	0.12	1.51	0.19	285.91	0.45	2.26	0.33
180.00	284.94	0.03	1.70	0.05	285.55	0.02	1.33	0.08

observed in MD simulation (Fig. 6). Comparable results were obtained by He *et al.* (2007) and Park *et al.* (2013) for HDTMA-montmorillonite organoclays. The same authors also observed a similar trend for the BE assigned to the C–C bond with a small shift of only 0.02 eV at small applied amounts of $HDTMA^+$ (up to 100% of the CEC) and larger shifts at greater applied amounts (up to 0.5 eV).

The second sub-peak contributing to the C 1s peak, assigned to the C–N bond, varied between 285.55 and 286.52 eV (Table 4). A larger variation of the C 1s BE in the C–N bonds in comparison to those of the C–C component (Fig. 5) might be explained by a larger impact of the positively charged pyridinium head group on the arrangement of the organic cations. Owing to the charge localization in the pyridinium ring, the head group is more sensitive to the environment and interacts more strongly than the aliphatic tail of the cations. The head groups interact electrostatically with the negative charge delocalized on the clay surface. At low loadings (<100% of the CEC) all organic cations interact directly with the surface as can be seen also from the MD simulations on the models with the monolayer arrangement (Fig. 5a–c, see below for discussion). In samples with greater cation loadings, the decreasing BEs indicate that some positively charged heads do not interact directly with the clay surface but are embedded between flexible aliphatic chains and imply a more complicated surface arrangement. Their excess positive charge is thus balanced by Cl^- ions trapped in their vicinity, which was confirmed by the survey XPS data (Fig. 2b). Therefore, different surface orientations are well reflected in the variation of the C 1s BE assigned to the C–N bonds (Fig. 5). These observations differ partially from results for HDTMA-montmorillonite (He *et al.*, 2007; Park *et al.*, 2013) where the variation in BE of the C–N sub-peak was minor (<0.12 eV). This difference can be attributed to the different head groups of the aromatic pyridinium ring in the $HDPy^+$ cation and the three methyl-groups bound to the N atom in the $HDTMA^+$ cation.

Molecular dynamics simulation

Figure 6 illustrates the last snapshots from the MD trajectories obtained after 5 ns of the production run for all eight models. The models HDPy_1 and HDPy_2 have one and two organic cations per computational cell, respectively, which corresponds to 33% and 67% of the CEC (Table 1). In these two models, some Na^+ ions remain to compensate the excess negative charge of the montmorillonite layer. In both cases the $HDPy^+$ ions have their aliphatic chains oriented nearly parallel to the surface forming a monomolecular surface layer. This surface arrangement is also confirmed with relatively simple and narrow peaks of the one-dimensional density profiles (ρ) of carbon atoms (Fig. 6a,b). In the HDPy_3 model (Fig. 6c) all surface Na^+ were substituted by $HDPy^+$ with a monomolecular arrangement in the initial configuration. This monomolecular arrangement is still preserved and all positively charged pyridinium heads are close to the clay surface with nearly the same distance from the plane of basal oxygen atoms. This is evident from one simple narrow peak of the one-dimensional density profile of the N atoms (Fig. 7c). Apart from the two previous models, the aliphatic chains have a more complicated arrangement on the surface. Mostly, they still form a monomolecular covering with the aliphatic chains parallel to the surface but it has already been observed that some aliphatic tails lose the parallel configuration by forming an incomplete and disordered second layer of aliphatic chains with tilted orientations and a varying conformation of the carbon chains (Fig. 7c). The movement of the aliphatic tails is quite intensive because of their flexibility and torsional variability of

https://doi.org/10.1180/claymin.2015.050.3.08 Published online by Cambridge University Press

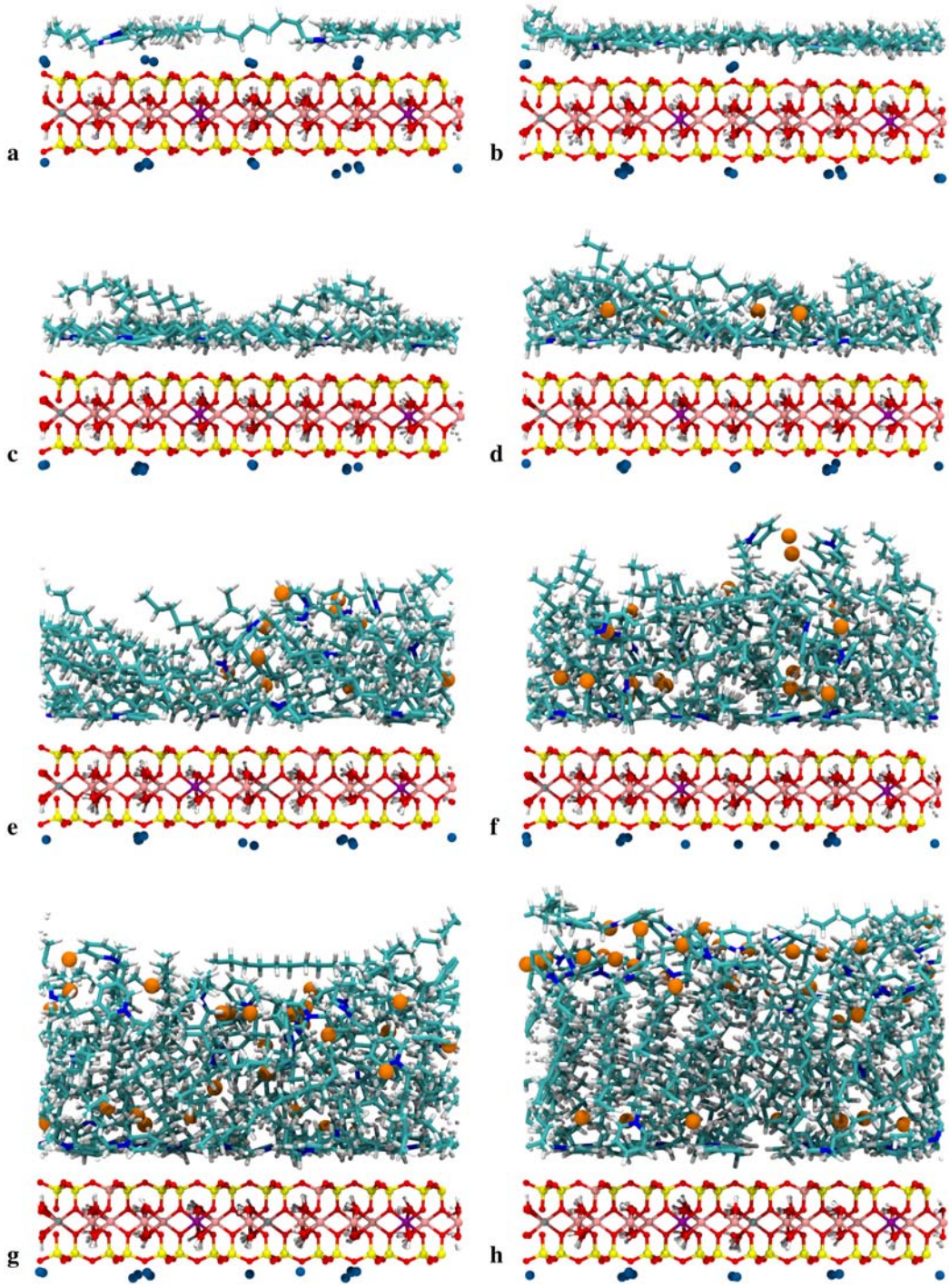

FIG. 6. Snapshots from MD simulations for studied models of HDPy-montmorillonites: (a) HDPy_1; (b) HDPy_2; (c) HDPy_3; (d) HDPy_4; (e) HDPy_6; (f) HDPy_8; (g) HDPy_10; and (h) HDPy_12 after 5 ns of *NVT* MD simulation. Blue spheres = Na^+; orange spheres = Cl^-.

https://doi.org/10.1180/claymin.2015.050.3.08 Published online by Cambridge University Press

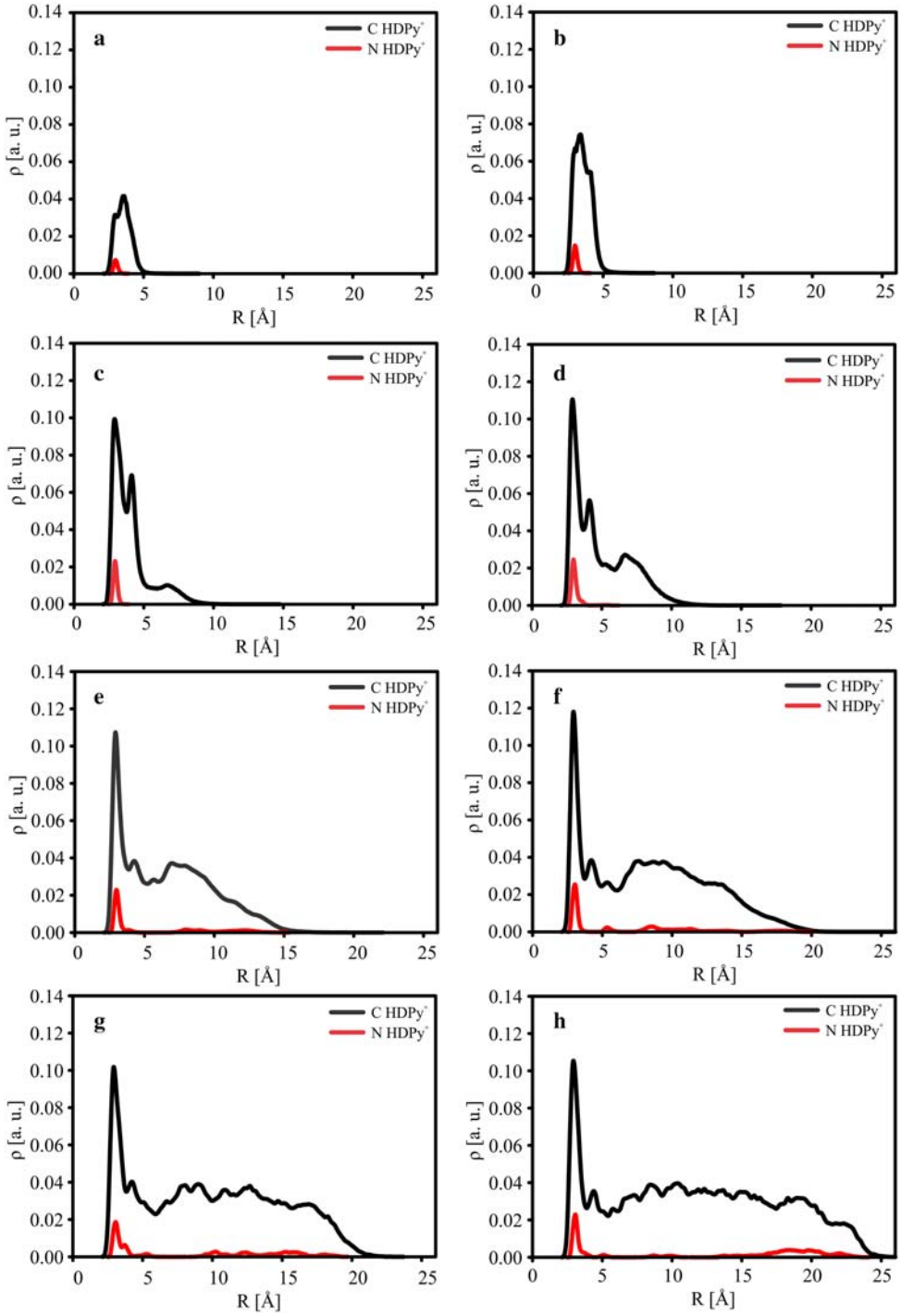

FIG. 7. One-dimensional atomic density profiles (ρ) for carbon and nitrogen atoms of organic cations calculated from MD simulations (5 ns, 300 K, *NVT* ensemble) for studied models of HDPy-montmorillonite: (a) HDPy_1; (b) HDPy_2; (c) HDPy_3; (d) HDPy_4; (e) HDPy_6; (f) HDPy_8; (g) HDPy_10; and (h) HDPy_12.

https://doi.org/10.1180/claymin.2015.050.3.08 Published online by Cambridge University Press

the C-chain. The surface arrangement of cations is even enhanced in the model with the initial monolayer arrangement (HDPy_4 in Fig. 6d). Although in this model the cation content exceeds the CEC (>100%), the positively charged heads are still located in the vicinity of the clay layer. This corresponds well to the one-dimensional density profile of the N atoms in Fig. 7d that still has the form of a single peak. The excess positive charge is compensated by Cl^- ions (dark yellow balls in Fig. 6) that are anchored close to one of the positively charged pyridinium rings. As the density of the long aliphatic chains on the surface increases, some of the chains are still quasi-parallel to the surface but most of them are clearly inclined to it. The thickness of the organic surface layer increases as it is documented by the increasing width of the one-dimensional density profile of the C atoms and the increasing intensity of the broad peak between 5 and 10 Å (Fig. 7d). The relationship between the total width of the C-density profiles and the number of the organic cations (Fig. 8) clearly shows a monolayer surface arrangement for the models with low cation loadings (1 and 2 organic cations in the original cell, Table 1) and the initiation of the more complicated surface arrangements with increasing cation density on the surface.

Molecular dynamics simulations on the models with the initial bilayer arrangement (6, 8, 10 and 12 organic cations in the original cell, Table 1) show a more complex cation distribution than the previous models. The positively charged head groups, which are localized near the surface in the initial configurations, remain stable in their positions due to strong electrostatic interactions with the negative charge of the clay mineral layer. Thus, a clear sharp peak at ~4 Å in the one-dimensional density profile of N atoms is evident in each of the plots in Fig. 6e–h. However, the expected second peak corresponding to the N atoms of the head groups oriented apart from the surface is not clear (Fig. 6e–h). This peak is 'delocalized' over a broad range and only in case of the greatest cation load (12 cations, model HDPy_12) is a broad peak in the range of 15–25 Å detected (Fig. 7h). Consequently, the results indicate that the arrangement of the organic cations is strongly disordered and difficult to identify as a regular bi- or multilayer surface arrangement. We interpret the results of MD simulations in such a way that some of the cations, mainly those with a positive head in the vicinity of the clay surface, have a parallel arrangement of the aliphatic chains with respect to the clay surface. The other cations have more complicated arrangements with the aliphatic chains in tilted positions with respect to the surface or with overcrossing chains in varying conformations due to their high flexibility and increasing density. Consequently, the width of the organic coating increases with the increasing cation content, as seen in the MD snapshots (Fig. 5e–h) and the corresponding one-dimensional density profiles of the C atoms (Fig. 6e–h). Only in case of the greatest cation density (HDPy_12) is it possible to interpret the surface arrangement of the cations as a very disordered paraffin-like configuration that differs from the more regular arrangement as described for the high organic cation content in the interlayer (e.g. He *et al.*, 2007; Heinz *et al.*, 2007). The total thickness of the organic cation coating increases regularly with the cation content (Fig. 8). For the greatest cation content, the total thickness of the first complete surface layer, consisting of the organic cation coating and a single montmorillonite layer, is ~25 Å. The results from the MD simulations correspond nicely with the interpretation based on XPS where the variation in C 1s BE of C–C and C–N bonds with the increasing organic cation content is in accord with the modelled surface orientations of the organic cations at external clay-mineral surfaces.

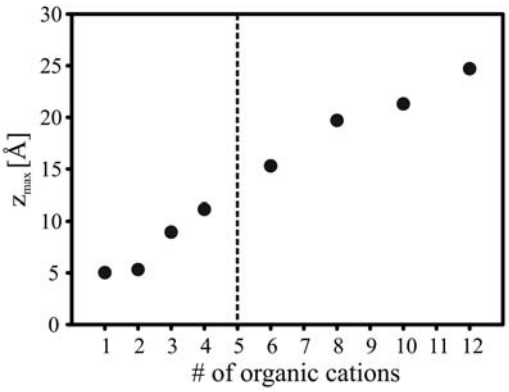

FIG. 8. Relationship between the total width of peaks, z_{max}, of ρ density profiles for C atoms (plus distance to the basal clay surface) and number of organic cations on the montmorillonite surface for HDPy_x models (where: x = 1–4, 6, 8, 10, and 12). Models on the left side of the dashed line had initial monolayer arrangements and, on the right side, bilayer).

SUMMARY AND CONCLUSIONS

The combination of XPS measurements and classical MD simulations provided complementary and

https://doi.org/10.1180/claymin.2015.050.3.08 Published online by Cambridge University Press

consistent insight into the orientation of the organic cations on the external surfaces of montmorillonite. The XPS-based surface element concentrations confirmed that $HDPy^+$ cations adsorbed upon release with exchangeable Na^+ and Ca^{2+} ions, but this exchange was incomplete at low organic cation loadings. At cation loadings exceeding 100% of the CEC, the Cl^- ions were increasingly incorporated for charge balance where, as shown by the MD simulations, they are primarily trapped in the vicinity of the positively charged cation heads. Variation in C 1s sub-peak BEs arising from C–C and C–N bonds reflected changes in the surface arrangement and conformations of organic cations at the surface and indicated new insights into organic-cation arrangement on the clay surface. For small surfactant uptakes, the organic cations were arranged as monolayers with a parallel orientation of the aliphatic chains to the clay surface and the electrostatic interactions between the positively charged heads and a delocalized negative charge of the clay mineral layers are dominant. With increasing organic cation content a disordered surface arrangement of the aliphatic chains begins to form with some of the aliphatic chains residing in an inclined configuration with respect to the surface. This differs from results obtained for the arrangement of organic cations in the clay interlayer which tend to be arranged more regularly (i.e. bi- or pseudotrimolecular). At high levels of surfactant uptake, a bilayer arrangement is formed, having positively charged heads of some of the organic cations in a very disordered second-layer arrangement. Molecular dynamics simulations confirmed these atomic-scale interactions and showed clearly the change from the mono- to disordered bilayer arrangement with the increasing surface coverage of the cations. For very high levels of uptake, quasi paraffin-like configurations were revealed. This study showed that the combination of experimental (XPS) and modelling (MD) methods represents a very effective tool for a detailed molecular-scale characterization of the arrangement of organic cations on the organoclay surfaces and the mechanism of their formation.

ACKNOWLEDGEMENTS

This study was supported under the D-A-CH collaboration of the Deutsche Forschungsgemeinschaft (DFG, German Research Foundation) under contract number SCHA 1732/1-1 and the FWF (Austrian Science Fund, Austria) under contract number I880-N21. The computational results presented were achieved using the Vienna Scientific Cluster (VSC).

REFERENCES

Bachmann J., Goebel M.-O. & Woche S.K. (2013) Small-scale contact angle mapping on undisturbed soil surfaces. *Journal of Hydrology and Hydromechanics*, **61**, 3–8.

Bilgic C., Yazici D.T., Karakehya N., Cetinkaya H., Singh A. & Chehimi M.M. (2014) Surface and interface physicochemical aspects of intercalated organo-bentonite. *International Journal of Adhesion Adhesives*, **50**, 204–210.

Böckenhoff K. & Fischer W.R. (2001) Determination of electrokinetic charge with a particle-charge detector, and its relationship to the total charge. *Fresenius Journal of Analytical Chemistry*, **371**, 670–674.

Cygan R.T., Liang J.J. & Kalinichev A.G. (2004) Molecular models of hydroxide, oxyhydroxide, and clay phases and the development of a general force field. *Journal of Physical Chemistry B*, **108**, 1255–1266.

Dultz S. & Bors J. (2000) Organophilic bentonites as adsorbents for radionuclides. II. Chemical and mineralogical properties of HDPy-montmorillonite. *Applied Clay Science*, **16**, 15–29.

Dultz S., Riebe B. & Bunnenberg C. (2005) Temperature effects on iodine adsorption on organo-clay minerals. II. Structural effects. *Applied Clay Science*, **28**, 17–30.

Fu Y.-T. & Heinz H. (2010) Cleavage energy of alkylammonium-modified montmorillonite and relation to exfoliation in nanocomposites: Influence of cation density, head group structure, and chain length. *Chemistry of Materials*, **22**, 1595–1605.

He H., Ding Z., Zhu J., Yan P., Xi Y., Yang D. & Frost R.L. (2005) Thermal characteristics of surfactant modified montmorillonites. *Clays and Clay Minerals*, **53**, 287–293.

He H., Zhou Q., Martens W.N., Kloprogge T.J., Yuan P., Xi Y., Zhu J. & Frost R.L. (2006) Microstructure of $HDTMA^+$-modified montmorillonite and its influence on sorption characteristics. *Clays and Clay Minerals*, **54**, 689–696.

He H., Zhou Q., Frost R.L., Wood B.J., Duong L.V. & Kloprogge T. (2007) A X-ray photoelectron spectroscopy study of HDTMAB distribution within organoclays. *Spectrochimica Acta Part A: Molecular and Biomolecular Spectroscopy*, **66**, 1180–1188.

He H., Ma Y., Zhu J., Yuan P. & Qing Y. (2010) Organoclays prepared from montmorillonites with different cation exchange capacity and surfactant configuration. *Applied Clay Science*, **48**, 67–72.

He H., Ma Y., Zhu J., Frost R.L., Theng B.K.G. & Bergaya F. (2014) Synthesis of organoclays: A critical review

https://doi.org/10.1180/claymin.2015.050.3.08 Published online by Cambridge University Press

and some unresolved issues. *Applied Clay Science*, **100**, 22–28.

Heinz H., Vaia R.A., Krishnamoorti R. & Farmer B.L. (2007) Self-assembly of alkylammonium chains on montmorillonite: Effect of chain length, head group structure, and cation exchange capacity. *Chemistry of Materials*, **19**, 59–68.

Heinz H., Vaia R.A. & Farmer B.L. (2008) Relation between packing density and thermal transitions of alkyl chains on layered silicate and metal surfaces. *Langmuir*, **24**, 3727–3733.

Hockney R.W. & Eastwood J.W. (1988) *Computer Simulation Using Particles.* Taylor & Francis Group, New York, pp. 18–22, 267–301.

Hoover W.G. (1985) Canonical dynamics: Equilibrium phase-space distributions. *Physical Review A*, **31**, 1695–1697.

Jagst E. (2010) *Surface Functional Group Characterization Using Chemical Derivatization X-ray Photoelectron Spectroscopy (CD-XPS)*. PhD thesis, Freie Universität Berlin, Germany.

Jorgensen W.L., Maxwell D.S. & Tirado-Rives J. (1996) Development and testing of the OPLS all-atom force field on conformational energetics and properties of organic liquids. *Journal of the American Chemical Society*, **118**, 11225–11236.

Klebow B. & Meleshyn A. (2012) Monte Carlo study of the adsorption and aggregation of alkyltrimethylammonium chloride on the montmorillonite-water interface. *Langmuir*, **28**, 13274–13283.

Koh S.M., Song M.S. & Takagi T. (2005) Mineralogy, chemical characteristics and stabilities of cetylpyridinium-exchanged smectite. *Clay Minerals*, **40**, 213–222.

Lee S.Y. & Kim S.J. (2002) Expansion characteristics of organoclay as a precursor to nanocomposites. *Colloids and Surfaces A: Physicochemical Engineering Aspects*, **211**, 19–26.

Lee S.Y., Cho W.J., Hahn P.S., Lee M., Lee Y.B. & Kim K.J. (2005) Microstructural changes of reference montmorillonites by cationic surfactants. *Applied Clay Science*, **30**, 174–180.

Li J., Zhu L. & Cai W. (2006) Characteristics of organobentonite prepared by microwave as a sorbent to organic contaminants in water. *Colloids and Surfaces A*, **281**, 177–183.

Meleshyn A. & Bunnenberg C. (2006) Interlayer expansion and mechanisms of anion sorption of Na-montmorillonite modified by cetylpyridinium chloride: A Monte Carlo study. *Journal of Physical Chemistry B*, **110**, 2271–2277.

Mravcakova M., Boukerma K., Omastova M. & Chehimi M.M. (2006) Montmorillonite/polypyrrole nanocomposites. The effect of organic modification of clay on chemical and electrical properties. *Material Science and Engineering C*, **26**, 306–313.

Naranjo P.B., Sham E.L., Rodriguez Castellon E., Torres Shanchez R.M. & Farfan Torres E.M. (2013) Identification and quantification of the interaction mechanisms between surfactant HDTMA-Br and montmorillonite. *Clays and Clay Minerals*, **61**, 98–106.

Park Y., Ayoko G.A. & Frost R.L. (2011) Application of organoclays for the adsorption of recalcitrant organic molecules from aqueous media. *Journal of Colloid and Interface Science*, **354**, 292–305.

Park Y., Ayoko G.A., Horvath E., Kurdi R., Kristof J. & Frost R.L. (2013) Structural characterisation and environmental application of organoclays for the removal of phenolic compounds. *Journal of Colloid and Interface Science*, **393**, 319–334.

Plimpton S. (1995) Fast parallel algorithms for short-range molecular dynamics. *Journal of Computational Physics*, **117**, 1–19.

Rytwo G., Gonen Y., Afuta S. & Dultz S. (2005) Interactions of pendimethalin with organo-montmorillonite complexes. *Applied Clay Science*, **28**, 67–77.

Rytwo G., Nir S. & Shuali U. (2012) Clay and water treatment. *Applied Clay Science*, **67–68**, 117–118.

Schampera B. & Dultz S. (2009) Determination of diffusive transport in HDPy-montmorillonite by H_2O-D_2O exchange using in situ ATR-FTIR spectroscopy. *Clay Minerals*, **44**, 249–266.

Schampera B. & Dultz S. (2011) The effect of surface charge and wettability on H_2O self diffusion in compacted clays. *Clays and Clay Minerals*, **59**, 42–57.

Shackelford C.D. & Moore S.M. (2013) Fickian diffusion of radionuclides for engineered containment barriers: Diffusion coefficients, porosities, and complicating issues. *Engineering Geology*, **152**, 133–147.

Sun H., Zhang J., Li L., Xu J. & Sun D. (2013) Surface modification of natural Na-montmorillonite in alkane solvents using a quaternary ammonium surfactant. *Colloids and Surfaces A: Physicochemical Engineering Aspects*, **426**, 26–32.

Tanuma S. (2003) Electron attenuation lengths. pp. 259–294 in: *Surface Analysis by Auger and X-ray Photoelectron Spectroscopy* (D. Briggs & J.T. Grant, editors). IM Publications, Chichester, UK and Surface Spectra Limited, Manchester UK.

Toma L.M., Gengler R.Y.N., Prinsen E.B., Gournis D. & Rudolf P. (2010) A Langmuir-Schaefer approach for the synthesis of highly ordered organoclay thin films. *Physical Chemistry Chemical Physics*, **12**, 12188–12197.

Van Reeuwijk L.P. (2003) *Procedures for Soil Analysis* (6th edition). ISRIC Technical paper 9. Wageningen, The Netherlands.

Yariv S. (2002) Introduction to organo-clay complexes and interactions. Pp. 39–122 in: *Organo-Clay Complexes and Interactions* (S. Yariv & H. Cross, editors). Marcel Dekker, New York, USA.

https://doi.org/10.1180/claymin.2015.050.3.08 Published online by Cambridge University Press

Zeng Q.H., Yu A.B., & Lu G.Q. (2004) Molecular dynamics simulation of the structural and dynamic properties of dioctadecyldimethylammonium in organoclays. *Journal of Physical Chemistry B*, **108**, 10025–10033.

Zhao Q. & Burns S.E. (2012) Molecular dynamics simulation of secondary sorption behavior of montmorillonite modified by single chain quaternary ammonium cations. *Environmental Science & Technology*, **46**, 3999–4007.

Zhao Q. & Burns S.E. (2013) Modelling sorption and diffusion of organic sorbate in hexadecyltrimethylammonium-modified clay nanopores – a molecular dynamics simulation study. *Environmental Science & Technology*, **47**, 2769–2776.

https://doi.org/10.1180/claymin.2015.050.3.08 Published online by Cambridge University Press